



## Flood Inundation Risk Analysis of Cascade Reservoirs Under Diverse Collapse Scenarios: A Two-Dimensional Hydrodynamic Modelling Approach



Meirong Jia<sup>⑩</sup>, Xiangyi Ding<sup>\*⑩</sup>, Junying Chu<sup>⑩</sup>, Xinyi Ma<sup>⑩</sup>, Xiaojie Tang<sup>⑩</sup>

State Key Laboratory of Simulation and Regulation of Water Cycle in River Basin, China Institute of Water Resources and Hydropower Research, 100038 Beijing, China

\* Correspondence: Xiangyi Ding (dingxy@iwhr.com)

Received: 01-04-2025

Revised: 03-20-2025

Accepted: 04-02-2025

**Citation:** M. R. Jia, X. Y. Ding, J. Y. Chu, X. Y. Ma, and X. J. Tang, "Flood inundation risk analysis of cascade reservoirs under diverse collapse scenarios: A two-dimensional hydrodynamic modelling approach," *J. Civ. Hydraul. Eng.*, vol. 3, no. 3, pp. 124–138, 2025. <https://doi.org/10.56578/jche030301>.



© 2025 by the author(s). Licensee Acadlore Publishing Services Limited, Hong Kong. This article can be downloaded for free, and reused and quoted with a citation of the original published version, under the CC BY 4.0 license.

**Abstract:** The risk of catastrophic flooding from sequential dam breaches in cascade reservoir systems has become increasingly critical under the influence of complex climate change and extreme geological events. In this study, a two-dimensional hydrodynamic dam-break model was developed to analyse flood propagation and inundation dynamics for the RE1, RE2, and RE3 cascade reservoirs in the lower Southwest China River Basin, considering various instantaneous full and partial collapse scenarios. Four distinct scenarios were simulated to evaluate breach characteristics and inundation impacts. Notably, Scenario 3-involving the simultaneous instantaneous full collapse of all three reservoirs-produced peak flow rates of 341,200 m<sup>3</sup>/s, 1,157,900 m<sup>3</sup>/s, and 340,100 m<sup>3</sup>/s at RE1, RE2, and RE3, respectively. Under this worst-case scenario, maximum inundation depths at representative sites A, B, C, and D reached 69.51 m, 79.87 m, 77.16 m, and 48.38 m, with high-severity flooding areas extending over 0.95 km<sup>2</sup>, 1.10 km<sup>2</sup>, 1.21 km<sup>2</sup>, and 1.73 km<sup>2</sup>, respectively. In comparison, Scenarios 1 and 2 generated lower peak flow rates, smaller inundation areas, and less severe flooding, while Scenario 4-representing overtopping without structural breach-resulted in a substantial reduction of high-risk zones. The findings highlight the pronounced escalation of flood risk under simultaneous multi-reservoir collapse conditions and underscore the necessity for enhanced coordinated flood management and emergency response strategies in cascade reservoir systems. This study offers valuable insights into dam failure risk assessment, contributing to improved flood mitigation policies and emergency preparedness in regions vulnerable to extreme hydrological events.

**Keywords:** Two-dimensional hydrodynamic modelling; Cascade reservoir system; Instantaneous full collapse; Partial collapse; Dam breach analysis; Flood risk assessment; Hydrologic Engineering Center-River Analysis System (HEC-RAS)

### 1 Introduction

Since the 1930s, the construction mode of cascade reservoirs has gradually emerged worldwide [1]. However, some dams developed earlier with lower design standards and prolonged operation periods now suffer from structural aging issues [2, 3]. Under extreme climate change and geological disaster scenarios, these dams are susceptible to breaching, thereby triggering basin-scale systemic risks that may result in incalculable life and property losses [4, 5]. In 1975, the sequential breaching of China's Banqiao and Shimantan large-scale reservoirs in Henan Province caused catastrophic consequences downstream, causing catastrophic consequences downstream, resulting in 26000 deaths and 11 million people affected by the disaster [6]. In 2020, the chain breaches of the Edenville and Sanford cascade dams in Michigan, USA inflicted massive losses on downstream industrial/agricultural production, resulting in approximately \$100 million in economic losses and forcing 11000 residents to evacuate urgently [7]. In 2023, storm-induced failures of the Mansour and Al-Bilad reservoirs in Derna, Libya resulted in nearly 100,000 casualties including missing persons in the city [8]. Floods triggered by cascade reservoirs breaches invariably cause exponentially greater damage to life and property downstream compared to single-dam failures [4]. Therefore, systematic analysis of cascading dam-break flood processes is of critical importance.

Currently available hydrodynamic models for dam-break simulation primarily include BREACH, DB-IWHR, Hydrologic Engineering Center-River Analysis System (HEC-RAS), and MIKE [9–11]. BREACH and DB-IWHR are based on parameterized breach development and specialize in simulating the progressive breach process of earth rock dams. However, they have limitations in calculating water flow coupling in complex terrains. MIKE is a commercial software that has the ability to simulate water sand structure coupling, but its computational resource consumption is significantly higher than open source tools. The HEC-RAS model supports two-dimensional unsteady flow calculation and is an open source software with good visualization effects, suitable for simulating flood breaches. Ma et al. [12] simulated the evolution process of the dam break flood in Daxin reservoir using MIKE21 software. Li et al. [13] established methodological integration between risk assessment approaches for cascade reservoirs and individual dams. Wang et al. [14] analyzed the accumulation and transmission processes of intrinsic and external risks during cascading dam failures. Wang et al. [15] compared and analyzed the applicability of the standard shallow water equation and the shallow water Boussinesq equation, and found that the Boussinesq model has good performance in downstream water depths. Říha et al. [16] used a shallow water hydrodynamic model to simulate the dam break flood paths of three cascade reservoirs and found that factors such as flood volume and slope have a significant impact on the attenuation effect of peak flow rate. Based on the current situation of cascade reservoir development in China, Wang et al. [17] analyzed the complexity of risk control for cascade reservoir dams. Liu et al. [10] coupled a one-dimensional flow model of a river channel with a DB-IWHR hyperbolic model to simulate the possibility of downstream reservoir failure caused by dam breaches in multiple upstream reservoirs. Liu [18] analyzed the flood transmission law of cascade reservoir groups under instantaneous horizontal and vertical outbursts. However, the interconnected effects among reservoirs in cascade configurations may amplify risks disproportionately [5]. Under different breach mode combinations, variations emerge in peak discharge, inundation extent, and flood severity. Current research on cascade reservoir failure risks under multi-mode breach combinations remains limited. Therefore, this study employs hydrodynamic modeling to simulate and analyze dam-break processes across various breach combination scenarios.

Focusing on the *RE1*, *RE2*, and *RE3* cascade reservoir system, this research develops a cascading breach model to elucidate hydraulic characteristics at breach sites and flood propagation mechanisms under different failure combinations. First, a two-dimensional dam-break model was constructed incorporating downstream topography, land use patterns, and reservoir parameters in the lower Southwest China River Basin. Second, numerical simulations under Scenarios 1-4 (varying breach combinations) revealed dynamic variations in flood discharge and water levels at dam axes. Finally, comparative analysis of maximum inundation depths and spatial extents across representative zones under these scenarios enabled quantitative assessment of flood severity. These findings provide references for operational management of cascade reservoirs under extreme flood conditions.

## 2 Methods

For cascade reservoir groups, the flow rate and water level variation processes during dam breaches exhibit significant complexity. Moreover, flood wave propagation patterns, affected areas, and temporal progression demonstrate marked differences across various breach scenarios. Given the advantages of high visualization and good computational accuracy of two-dimensional hydrodynamic models, this section establishes a 2D hydrodynamic cascade reservoir breach model. First, potential breach typologies are systematically categorized. Subsequently, quantitative assessment metrics for flood severity are established.

### 2.1 Model Principle Analysis

The adopted dam-break model features a hybrid parametric-physical architecture. In this model, a parameterized model is used to predict the final breach parameters, and a simplified physical breach mechanism is introduced to calculate the outflow process of the breach. When simulating the process of breach discharge, the outflow from the breach is in the form of a wide topped weir. The flow calculation formula is as follows [19, 20]:

$$Q_n = CL_n Z_n^{3/2} \quad (1)$$

where,  $Q_n$  represents the cross-sectional discharge at the  $n^{th}$  reservoir ( $\text{m}^3/\text{s}$ );  $C$  denotes the weir flow coefficient;  $L_n$  indicates the weir length of the  $n^{th}$  reservoir (m);  $Z_n$  stands for the head over the weir crest of the  $n^{th}$  reservoir (m).

In the computational analysis of two-dimensional dam-break flood propagation induced by overtopping, the two-dimensional unsteady flow simulation employs the simplified two-dimensional form of the Navier-Stokes equations—specifically, the shallow water equations. Its applicability depends on the assumptions of static water pressure distribution, horizontal scale being much larger than vertical scale, and vertical velocity being negligible. It is suitable for large-scale slow flow scenarios such as river channels, floodplains, reservoirs, etc., such as flood routing, water conservancy engineering design, and surface water simulation. However, this equation has limitations when there is significant vertical acceleration (such as waterfalls, water jumps), non-hydrostatic pressure distribution, or

stratified flow, and complex terrain or rapids may lead to numerical instability. The upstream boundary conditions need to be reasonably set for flow/water level input, initial state (such as terrain data, Manning roughness), and internal structural parameters (dam, gate). The downstream boundary condition is based on the normal depth. Under the assumption of incompressible flow conditions, the governing equations consisting of the continuity equation and momentum equations can be expressed as [21].

Continuity equations:

$$\frac{\partial H}{\partial t} + \nabla \cdot hV + q = 0 \quad (2)$$

Momentum equation:

$$\frac{\partial V}{\partial t} + V \cdot \nabla V = -g\nabla H + v_t \nabla^2 V - c_f V + fk \times V \quad (3)$$

where,  $H$  is the water surface elevation (m);  $h$  is the water depth (m);  $V$  is the flow velocity (m/s);  $Q$  is the lateral inflow ( $\text{m}^3/\text{s}$ );  $t$  is time (s);  $v_t$  is the viscosity coefficient of horizontal motion ( $\text{m}^2/\text{s}$ ), taking an empirical value of  $0.1 \sim 0.5 \text{ m}^2/\text{s}$ ;  $c_f$  is the coefficient of friction at the bottom of the riverbed, taken as 0.0025;  $g$  is the gravity acceleration ( $\text{m}/\text{s}^2$ ), taken as  $9.8 \text{ m}/\text{s}^2$ ;  $f$  is the Coriolis parameter, ignoring the influence of Earth's rotation and taking 0;  $k$  is the vertical unit vector.

## 2.2 Classification of Possible Breaches

In extreme flood situations, gates may malfunction [22]. Therefore, this study adopts a fault overflow collapse chain hypothesis framework, assuming that all flood discharge gates are completely locked due to faults. This setting may overestimate the initial water level rise rate, but it can cover the most unfavorable situation and is suitable for the development of flood control emergency plans. Based on statistical data analysis, overtopping is the main mode of failure that causes dam collapse, so it is assumed that the failure mode is overtopping. Concrete dams have high material strength and good consistency, and are generally less prone to collapse. However, under extreme weather and geological disasters, concrete dams may collapse in a very short period of time, affecting the safety of downstream people's lives and property. In practical engineering, the possible failure modes of concrete dams mainly include instantaneous partial failure and instantaneous full failure. In cascade reservoirs consisting of  $n$  reservoirs, there are several possible failure combination patterns that may occur. Taking the situation of three reservoirs as an example, the possible scenarios of cascade reservoir group collapse are shown in Table 1.

**Table 1.** Cascade reservoir collapse scenario

Collapse Scenario	Reservoir Breach Mode		
Scenario <i>a</i>	$RE1 \rightarrow$	$RE2 \rightarrow$	$RE3 \rightarrow$
Scenario <i>b</i>	$RE1 \rightarrow$	$RE2 \rightarrow$	$RE3 \downarrow$
Scenario <i>c</i>	$RE1 \rightarrow$	$RE2 \downarrow$	$RE3 \downarrow$
Scenario <i>d</i>	$RE1 \rightarrow$	$RE2 \downarrow$	$RE3 \rightarrow$
Scenario <i>e</i>	$RE1 \downarrow$	$RE2 \rightarrow$	$RE3 \rightarrow$
Scenario <i>f</i>	$RE1 \downarrow$	$RE2 \rightarrow$	$RE3 \downarrow$
Scenario <i>g</i>	$RE1 \downarrow$	$RE2 \downarrow$	$RE3 \rightarrow$
Scenario <i>h</i>	$RE1 \downarrow$	$RE2 \downarrow$	$RE3 \downarrow$

Note:  $\rightarrow$  indicates instantaneous partial collapse;  $\downarrow$  indicates instantaneous full collapse.

## 2.3 Severity of Dam Break Floods

The depth and velocity of floods are the main indicators for measuring the impact of dam break floods. According to the product of water depth and flow velocity ( $D \cdot V$ ), the severity of dam break floods can be classified into low, medium, and high severity levels, as shown in Table 2.

**Table 2.** Classification of flood severity

Severity of Floods	$D \cdot V$
Low severity	$D \cdot V < 4.6 \text{ m}^2/\text{s}$
Moderate severity	$4.6 \text{ m}^2/\text{s} \leq D \cdot V \leq 12 \text{ m}^2/\text{s}$
High severity	$D \cdot V > 12 \text{ m}^2/\text{s}$

### 3 Case Analysis

#### 3.1 Overview of the Research Area

Taking three consecutive reservoirs (*RE1*, *RE2*, and *RE3*) within the study basin as an example, the main parameters of each reservoir are shown in Table 3. In the Southwest China River Basin, reservoir *RE2* has large regulating storage capacity and is responsible for flood control tasks [23, 24]. The upstream catchment areas of *RE1*, *RE2*, and *RE3* reservoirs are approximately 136,000, 116,400, and 127,624 km<sup>2</sup>, respectively. The research basin belongs to the climate zone of the western Sichuan Plateau, and is influenced by the high-altitude westerly circulation and southwest monsoon, with distinct dry and wet seasons. The rainy season is from May to October, accounting for 90% -95% of the annual rainfall. Large scale rainstorm occurs in the basin from June to September, mainly in July and August. Due to the low rainfall intensity in most areas of the basin and the narrow strip shape of the basin, it is not conducive to flood collection. Therefore, floods in this basin generally have characteristics such as relatively low peak, large volume, and long duration. The river reach associated with this cascade reservoir system belongs to a mountainous river, and the channel roughness was determined with reference to empirical values for mountainous channel roughness and natural channel roughness tables. The schematic diagram of the cascade reservoir is shown in Figure 1.

**Table 3.** Basic parameters of reservoirs

Reservoir	Total Storage Capacity ( $\times 10^7$ m <sup>3</sup> )	Dam Height (m)	Normal Storage Level (m)	Dead Water Level (m)
RE1	76.00	168.0	1330	1321
RE2	580.00	240.0	1200	1155
RE3	9.12	69.5	1015	1012

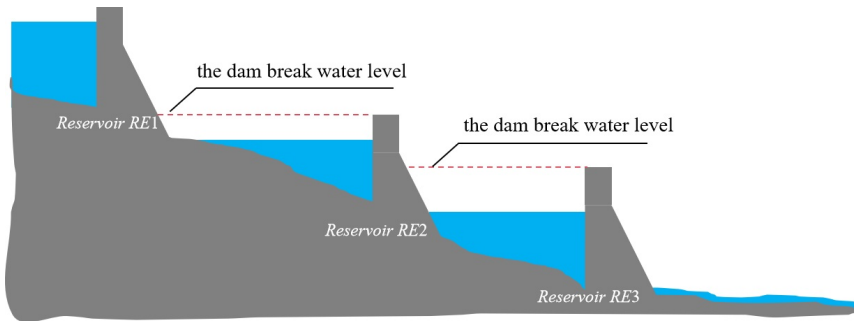


**Figure 1.** Schematic diagram of cascade reservoir

#### 3.2 Classification of Collapse Scenarios

This study assumes that the gates and flood discharge structures cannot be opened due to malfunctions, resulting in the inability of the reservoir to discharge water normally and causing dam collapse after overflowing. The width of the breach in the instant total collapse mode is the total length of the main dam, and the height of the breach is the height of the main dam. In the instant partial breach mode, the final bottom width of the breach is half of the length of the main dam, and the height of the breach is the height of the main dam. Based on the impact and damage situation after dam failure, the following four failure scenarios were selected for research, as shown in Table 4.

**Table 4.** Cascade reservoir collapse scenario of the Southwest China River downstream

Collapse Scenario	Reservoir Breach Mode		
Scenario 1	<i>RE1</i> →	<i>RE2</i> →	<i>RE3</i> →
Scenario 2	<i>RE1</i> ↓	<i>RE2</i> →	<i>RE3</i> ↓
Scenario 3	<i>RE1</i> ↓	<i>RE2</i> ↓	<i>RE3</i> ↓
Scenario 4	<i>RE1</i>	<i>RE2</i>	<i>RE3</i>

Scenario 1: The reservoirs *RE1*, *RE2*, and *RE3* all experienced instantaneous partial collapse.

Scenario 2: Both the reservoirs *RE1* and *RE3* experienced an instantaneous full collapse, while reservoir *RE2* experienced an instantaneous partial collapse.

Scenario 3: The reservoirs  $RE1$ ,  $RE2$ , and  $RE3$  all experienced instantaneous full collapse.

Scenario 4: Reservoirs  $RE1$ ,  $RE2$ , and  $RE3$  will not experience a breach.

### 3.3 Model Construction and Result Analysis

#### 3.3.1 Model construction

The elevation of the land terrain is sourced from the ASF website NASA Synthetic Aperture Radar data ASTER GDEM V2, with a spatial resolution of approximately  $12.5 \text{ m} \times 12.5 \text{ m}$ . In the modeling process, three linear reservoirs and control basins were mainly set up. Linear reservoir assumes a linear relationship between reservoir storage capacity and outflow. Set the control basin as a two-dimensional grid area and increase the grid density at the reservoir connection.

Due to the large research area, the grid density is set to  $20 \text{ m} \times 20 \text{ m}$ , with a total of approximately 1.26 million grids. This study assumes that overtopping leads to dam failure, meaning that when the water level of the reservoir exceeds the elevation of the dam crest, the dam body will collapse. Due to the absence of reservoir dam failure events in the basin, the upstream boundary is designed for a flood process that occurs once every 5000 years, and the downstream boundary conditions are based on a natural riverbed gradient of  $2.32\%$  downstream of the river channel. The initial flow rate of the river channel is set at  $1000 \text{ m}^3/\text{s}$ .

#### 3.3.2 Model validation

In the Southwest China River Basin, reservoirs  $RE1$ ,  $RE2$ , and  $RE3$  have been put into operation, but the cascade reservoirs have not actually experienced any dam failure accidents, and there is no measured data on dam failure floods. To verify the correctness of the established model, a flood process that occurred within the period of 7/1 to 8/29 in two years was selected for simulation, and the simulation results were compared with the measured results of a hydrological station. The results are shown in Figure 2.

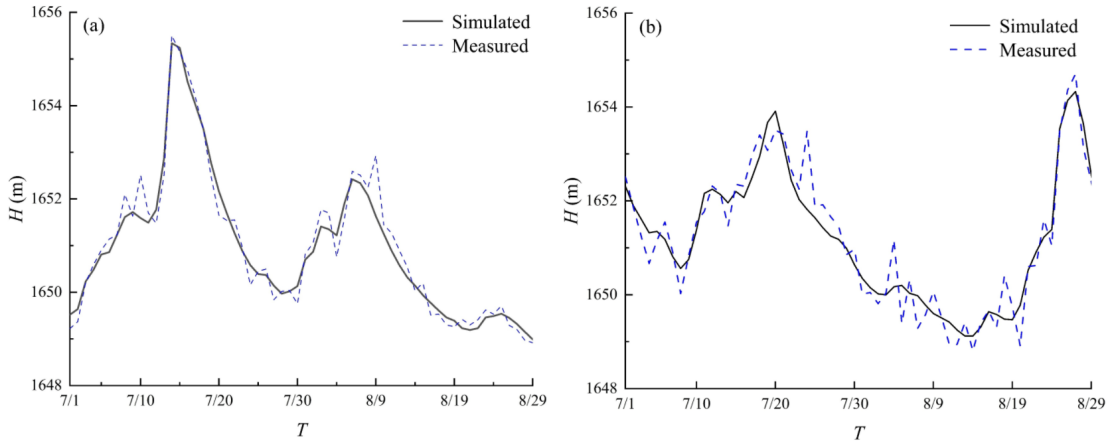


**Figure 2.** Comparison of measured and simulated water level changes at hydrological stations

According to subgraph (a) of Figure 2, during the selected time period, the measured results of the hydrological station showed two water level peaks, namely  $1655.34 \text{ m}$  and  $1652.42 \text{ m}$ . And the simulated water level also showed two peaks,  $1655.50 \text{ m}$  and  $1652.93 \text{ m}$ . In Figure 2, the difference between the first and second peak water levels measured and simulated is only  $0.16 \text{ m}$  and  $0.51 \text{ m}$ , respectively, which is relatively small. According to subgraph (b) of Figure 2, during the selected time period, the measured results of the hydrological station showed two water level peaks, namely  $1653.91 \text{ m}$  and  $1654.33 \text{ m}$ . And the simulated water level also showed two peaks, namely  $1653.51 \text{ m}$  and  $1654.70 \text{ m}$ . In subgraph (b) of Figure 2, the difference between the first and second peak water levels measured and simulated is only  $0.40 \text{ m}$  and  $0.37 \text{ m}$ , respectively, which is relatively small. Moreover, in Figure 2, the trend of changes in simulated and measured water levels is also relatively close. Therefore, the model established in this article can reflect the overcurrent process in the selected river channel and can be used for subsequent research on dam break flood simulation.

#### 3.3.3 Water level and flow rate at the breach

In Scenarios 1-4, the evolution process of dam break floods in the  $RE1$ ,  $RE2$ , and  $RE3$  cascade reservoirs was simulated using hydrodynamic models.

##### (1) Scenario 1

In Scenario 1, the changes in water level and flow rate at each reservoir breach are shown in Figure 3.

According to Figure 3, when all three reservoirs experienced instantaneous partial collapse, the peak flow rate of the reservoir  $RE1$  after the dam breach was  $230,200 \text{ m}^3/\text{s}$ , and the highest water level reached  $1,332.87 \text{ m}$ . Due to

the distance between reservoir  $RE_2$  and reservoir  $RE_1$ , and the large storage capacity of  $RE_2$  reservoir, the required storage time for reservoir  $RE_2$  is longer, and the dam failure time is later. About 40.0 hours after the collapse of reservoir  $RE_1$ , reservoir  $RE_2$  experienced a dam failure. After the dam breach, the flow rate at the breach showed a trend of first increasing and then decreasing, with a peak flow rate of 656,000 m<sup>3</sup>/s and a maximum water level of 1,201.94 m. About 4.6 hours later, the reservoir  $RE_3$  experienced a dam failure, with a peak flow rate of 109,100 m<sup>3</sup>/s and a maximum water level of 1,015.75 m.

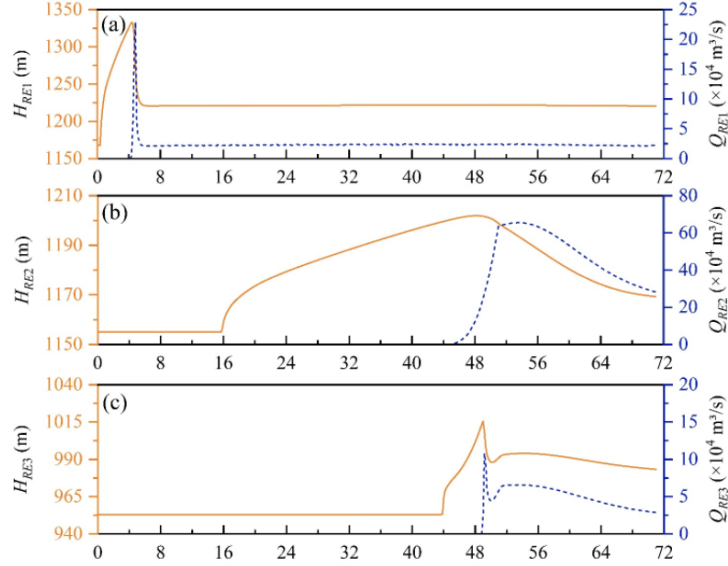


**Figure 3.** Variations in water levels and flow rates at the breach of reservoirs (a)  $RE_1$ , (b)  $RE_2$ , and (c)  $RE_3$  under Scenario 1

## (2) Scenario 2

In Scenario 2, the changes in water level and flow rate at each reservoir breach are shown in Figure 4.

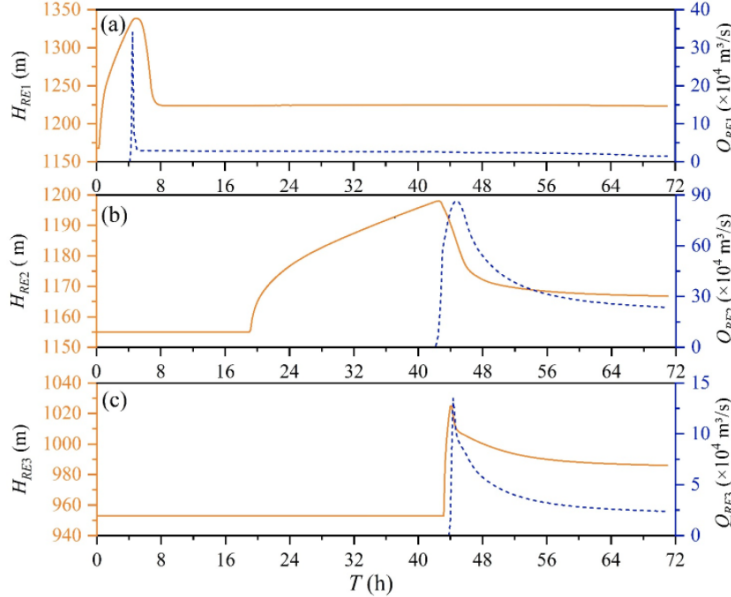


**Figure 4.** Variations in water levels and flow rates at the breach of reservoirs (a)  $RE_1$ , (b)  $RE_2$ , and (c)  $RE_3$  under Scenario 2

According to Figure 4, when the reservoir  $RE_2$  experiences an instantaneous partial collapse and other reservoirs experience an instantaneous full collapse, the peak flow rate of the reservoir  $RE_1$  after the dam break is 341,200 m<sup>3</sup>/s, and the highest water level reaches 1,338.59 m. After 37.8 hours of dam failure in a reservoir, reservoir  $RE_2$  began to experience dam failure. With the continuous development of the breach, the peak flow rate of the breach

reached 864,600 m<sup>3</sup>/s, and the highest water level reached 1,198.04 m. After the collapse of reservoir *RE*2, the dam breach flood spread to reservoir *RE*3. Due to the small storage capacity of reservoir *RE*3, a dam breach occurred before the upstream reservoir *RE*2 reached its peak flow rate. The peak flow rate of the dam breach was 135,700 m<sup>3</sup>/s, and the highest water level reached 1,025.47 m.

#### (3) Scenario 3

In Scenario 3, the changes in water level and flow rate at each reservoir breach are shown in Figure 5.

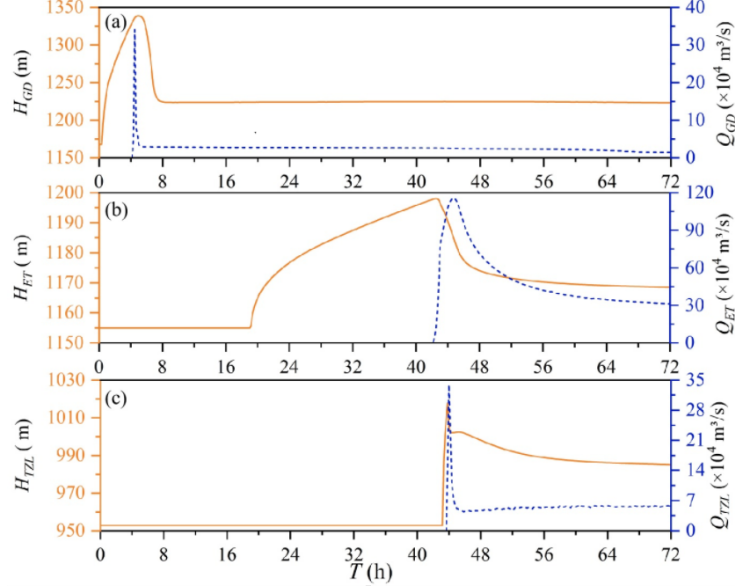


**Figure 5.** Variations in water levels and flow rates at the breach of reservoirs (a) *RE*1, (b) *RE*2, and (c) *RE*3 under Scenario 3

According to Figure 5, when all three reservoirs collapsed instantly, the peak flow rate of the reservoir *RE*1 dam breach was 341,200 m<sup>3</sup>/s, and the highest water level reached 1,338.91 m. After 37.7 hours of dam failure in reservoir *RE*1, reservoir *RE*2 began to collapse, with a peak flow rate of 1,157,900 m<sup>3</sup>/s and a maximum water level of 1,198.14 m. After 1.8 hours of dam failure in reservoir *RE*2, reservoir *RE*3 began to collapse, with a peak flow of 340,100 m<sup>3</sup>/s and a maximum water level of 1,017.78 m.

#### (4) Scenario 4

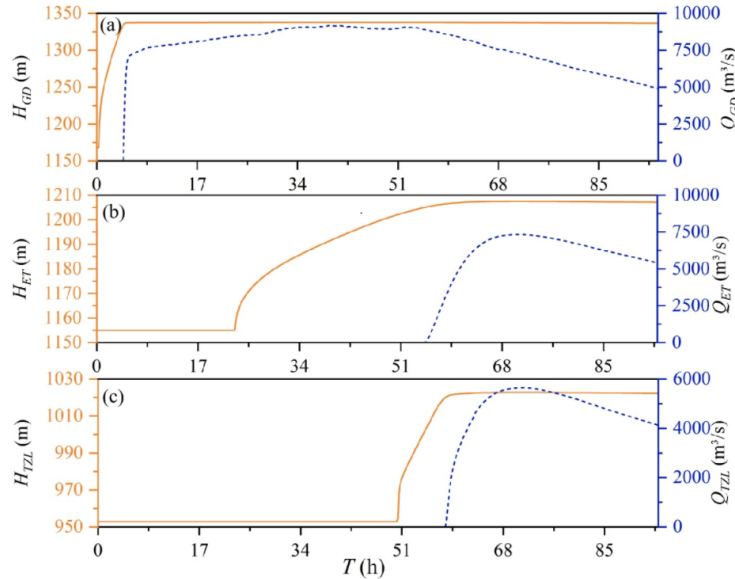


**Figure 6.** Variations in water levels and flow rates at the reservoirs (a) *RE*1, (b) *RE*2, and (c) *RE*3 under Scenario 4

In Scenario 4, the changes in water level and flow rate at each reservoir breach are shown in Figure 6.

According to Figure 6, when none of the three reservoirs experienced a breach, the peak flow rate of reservoir *RE1* was  $9,618 \text{ m}^3/\text{s}$ , and the highest water level reached 1,337.59 m. The peak flow rate of reservoir *RE2* reached  $7,331.3 \text{ m}^3/\text{s}$ , and the highest water level reached 1,207.48 m. The peak flow rate of reservoir *RE3* is  $5,640.6 \text{ m}^3/\text{s}$ , and the highest water level reaches 1,022.74 m.

From Figures 3 and 4, it can be seen that in Scenarios 1 and 2, the reservoir *RE1* experienced instantaneous partial collapse and instantaneous full collapse, respectively, resulting in significant differences in its dam-breaking flood process. The peak flow rates reached  $230,200 \text{ m}^3/\text{s}$  and  $341,200 \text{ m}^3/\text{s}$ , respectively, which led to changes in the water storage process of the reservoir *RE2*. In Scenario 2, the water level of reservoir *RE1* rises faster, the storage time becomes shorter, and the dam failure time is advanced. And its peak flow rate due to dam failure reached  $864,600 \text{ m}^3/\text{s}$ , far greater than the  $656,000 \text{ m}^3/\text{s}$  in Scenario 1. Correspondingly, this has led to an earlier dam failure time for the downstream reservoir *RE3* and an increase in peak dam failure flow. From Figures 3 and 5, it can be seen that in Scenarios 1 and 3, reservoirs *RE1*, *RE2*, and *RE3* experienced instantaneous partial collapse and instantaneous full collapse, respectively. In Scenario 3, the peak flow rates of each reservoir breach are  $341,200 \text{ m}^3/\text{s}$ ,  $1,157,900 \text{ m}^3/\text{s}$ , and  $340,100 \text{ m}^3/\text{s}$ , respectively, which are much higher than Scenario 1. Moreover, the dam breach time of downstream reservoirs *RE2* and *RE3* has been advanced, which is the most unfavorable. In Scenario 4, it is evident that the peak and highest water level occur relatively late, and the highest water level is relatively higher, which can effectively store floods and ensure downstream safety. Therefore, if the cascade reservoirs of *RE1*, *RE2*, and *RE3* collapse, efforts should be made to avoid the adverse situation of instantaneous full collapse in all three reservoirs.

To compare the breach flow process of a single reservoir encountering over standard floods and upstream floods in a cascade reservoir group, this study simulated the breach process of a single reservoir with instantaneous full collapse and instantaneous partial collapse. The peak flow rate is shown in Table 5.

**Table 5.** Peak flow rate of a single reservoir in case of instantaneous partial and full collapse

Reservoir	Peak Flow Rate ( $\text{m}^3/\text{s}$ )	
	Instantaneous partial collapse	Instantaneous full collapse
<i>RE1</i>	230,200	341,200
<i>RE2</i>	505,500	681,200
<i>RE3</i>	92,900	162,200

Due to the fact that the reservoir *RE1* is the first reservoir of the cascade reservoir group, the peak flow rate of dam failure is not affected by the linkage of the cascade reservoirs. Therefore, in Table 5, the peak flow rate at the breach point of reservoir *RE1* is the same when the dam breaks alone or when there is an instantaneous full or partial collapse in cascade reservoirs. According to Table 5, when the reservoir *RE2* experiences an instantaneous partial collapse, the peak flow rate of the dam failure is  $505,500 \text{ m}^3/\text{s}$ . In the cascade reservoirs mode, when both reservoirs *RE1* and *RE2* experienced instantaneous partial collapse, the peak flow rate of reservoir *RE2* dam failure reached  $656,000 \text{ m}^3/\text{s}$ . Compared with the operation mode of cascade reservoirs, the peak flow rate of reservoir *RE2* when it collapses alone is smaller. Similarly, in the single reservoir mode, the peak flow rate of the reservoir *RE2* reached  $681,200 \text{ m}^3/\text{s}$  when it experienced an instantaneous full collapse. Only slightly larger than the situation where all cascade reservoirs experience instantaneous partial collapse (Scenario 1), and significantly smaller than the peak flow rate of dam failure ( $1,157,900 \text{ m}^3/\text{s}$ ) in the case where all cascade reservoirs experience instantaneous full collapse (Scenario 3). Similarly, in the single reservoir mode, the peak flow rate during the instantaneous partial collapse and instantaneous full collapse of reservoir *RE3* is smaller than in the cascade reservoirs mode. The results indicate that the hydraulic correlation between cascade reservoirs leads to the superposition effect of floods, resulting in a larger and more unfavorable peak flow rate in the cascade reservoirs mode compared to the single reservoir mode.

### 3.3.4 Submergence degree of dam break flood

This study combined hydrodynamic models and ArcGIS software to establish a map of the depth and degree of flood inundation caused by dam failure in cascade reservoirs. In the ICOLD Guidelines for Flood Risk Assessment, population density is identified as the primary risk factor. Therefore, the most densely populated areas downstream of each reservoir in the cascade reservoir group were selected to analyze their inundation situation, in order to conduct risk assessment and develop corresponding escape routes for subsequent research. The representative locations of each inundation are A (Baru Township, Xichang City), B (Fangtian Township, Miyi County), C (Tongzilin Town, Yanbian County), and D (Yimin Township and Jinjiang Town), as shown in Figure 7. In Scenarios 1-4, the flood inundation depth and degree at each flood inundation representative point were analyzed separately, achieving visualization of the risk distribution of dam failure in cascade reservoirs.

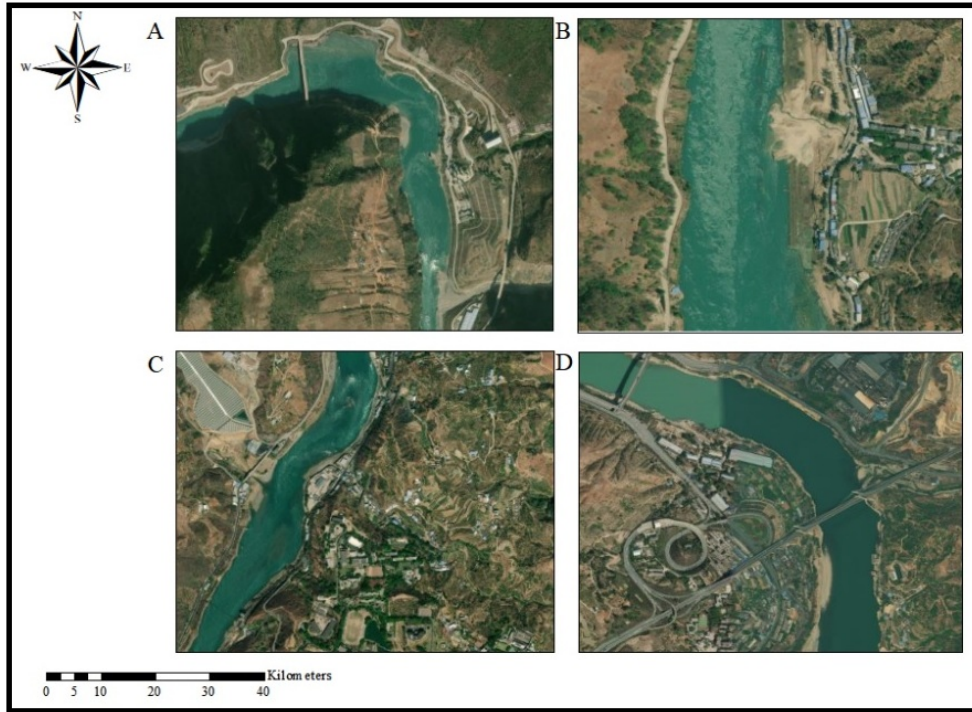


**Figure 7.** Flood inundation points of cascade reservoirs

### (1) Scenario 1

In Scenario 1, the flood inundation situation and degree of inundation of representative locations A, B, C, and D are shown in Figures 8 and 9, respectively.

From Figure 8, it can be seen that in Scenario 1, the submerged representative locations A, B, and C reached maximum submerged depths of 64.77, 68.18, and 62.53 m, respectively. Compared to the other three locations, location D is located at the furthest downstream and has a wider river channel. When the flood flows through this area, there is a wider river channel to pass through, and the water depth inside the river channel is smaller. Therefore, the average water depth at location D is smaller, with a maximum submergence depth of only 44.79 m. From Figure 9, it can be seen that when a flood occurs, the submerged areas at representative locations A, B, C, and D gradually increase, reaching a submerged area of 0.91, 1.12, 1.36, and 1.77 km<sup>2</sup>, respectively. The reason is that, generally speaking, the closer to the downstream, the smaller the slope of the river channel and the wider the river channel. Therefore, the submerged area at location D is the largest. Moreover, according to the classification criteria described in Table 2, the vast majority of the submerged areas in these four locations exhibit a high degree of severe flooding. At the representative location D of inundation, the area of the high severity zone is the largest, reaching 1.57 km<sup>2</sup>.

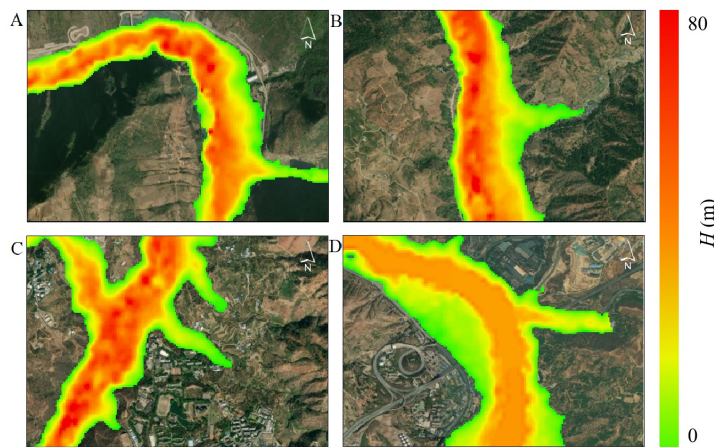


**Figure 8.** Flood depth of representative inundation locations A, B, C, and D under Scenario 1

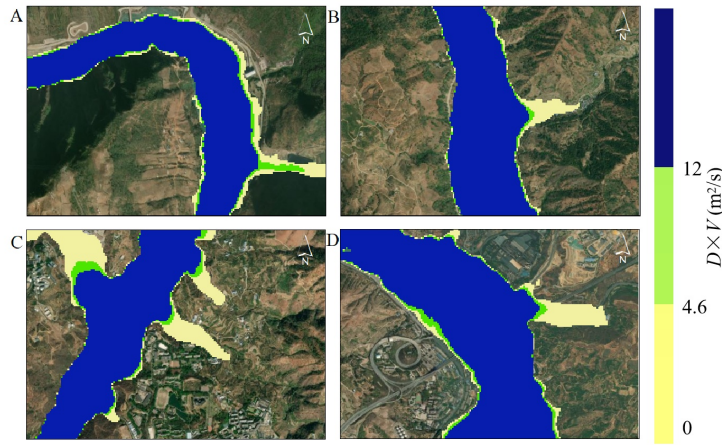


**Figure 9.** Flood inundation degree of representative locations A, B, C, and D under Scenario 1

## (2) Scenario 2

In Scenario 2, the flood inundation situation and degree of inundation of representative locations A, B, C, and D are shown in Figures 10 and 11, respectively.

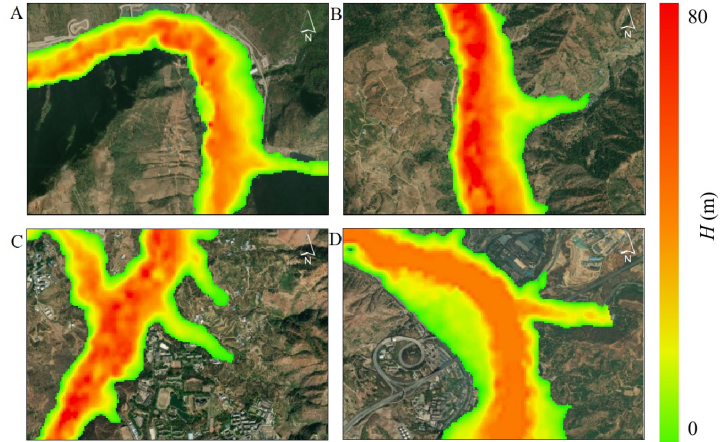


**Figure 10.** Flood depth of representative inundation locations A, B, C, and D under Scenario 2

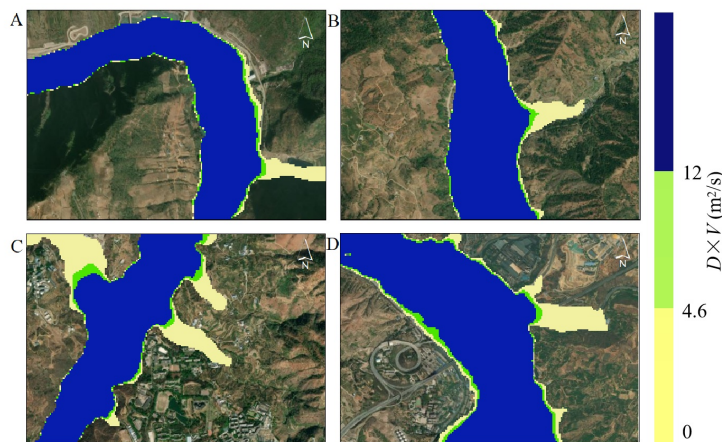


**Figure 11.** Flood inundation degree of representative locations A, B, C, and D under Scenario 2

As shown in Figure 10, in Scenario 2, the submerged areas at representative locations A, B, C, and D gradually increase, reaching 1.05, 1.16, 1.53, and 1.96 km<sup>2</sup>, respectively. Similarly, the maximum submergence depth at

location D is smaller than that at locations A, B, and C, at only 48.78 m. At locations A, B, and C, the maximum submergence depths reached 69.51, 73.09, and 67.35 m, respectively. From Figure 11, it can be seen that in these four areas, the vast majority of the submerged areas exhibit high severity. At location A, there is a high-severity area of 0.89 km<sup>2</sup>, and a total area of 0.1 km<sup>2</sup> for moderate and low-severity areas. The high severity area at location B is 1.05 km<sup>2</sup>. At location C, the high severity area covers 1.09 km<sup>2</sup>, while the moderate and low severity areas together cover 0.44 km<sup>2</sup>. At location D, the area of high-severity area is the largest, reaching 1.64 km<sup>2</sup>, which is the most severe.

### (3) Scenario 3

In Scenario 3, the flood inundation situation and degree of inundation of representative locations A, B, C, and D are shown in Figures 12 and 13, respectively.

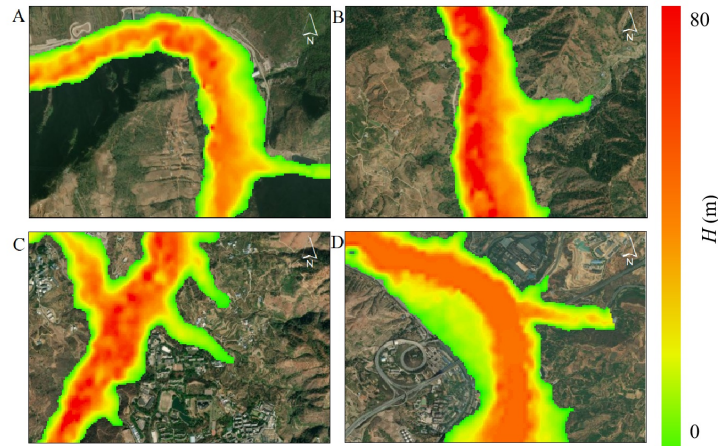


**Figure 12.** Flood depth of representative inundation locations A, B, C, and D under Scenario 3

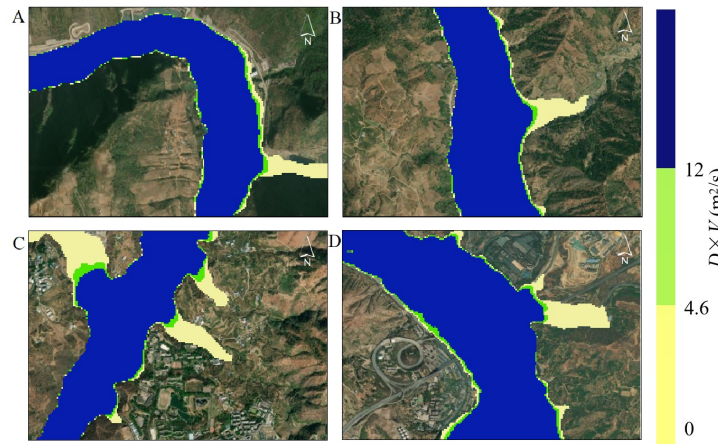


**Figure 13.** Flood inundation degree of representative locations A, B, C, and D under Scenario 3

In Scenario 3, all three reservoirs experienced an instantaneous full collapse. According to Figure 12, the maximum submergence depth at representative locations B and C is the highest, reaching 79.87 and 77.16 m respectively. Next is the submerged representative location A, which is 69.51 m. The maximum submergence depth at location D is the smallest, at 48.38 m. Similar to Scenarios 1 and 2, the submerged area gradually increases at representative locations A, B, C, and D. At location D, the submerged area is the largest, reaching 2.05 km<sup>2</sup>. The submerged area at location A is the smallest, only 1.05 km<sup>2</sup>. Similarly, due to the high water depth and flow velocity, the vast majority of the submerged areas at representative locations A, B, C, and D have shown a high severity of flooding. Due to the gradual increase in the inundation area at representative locations A, B, C, and D, the area of high-severity areas at each location also gradually increases. At location D, the area of high-severity area is the largest, reaching 1.73 km<sup>2</sup>. In Scenario 3, the maximum submergence depth at location B is the largest, and the area of high-severity zone at location D is the largest, which is relatively unfavorable.

### (4) Scenario 4

In Scenario 4, the flood inundation situation and degree of inundation of representative locations A, B, C, and D are shown in Figures 14 and 15, respectively.

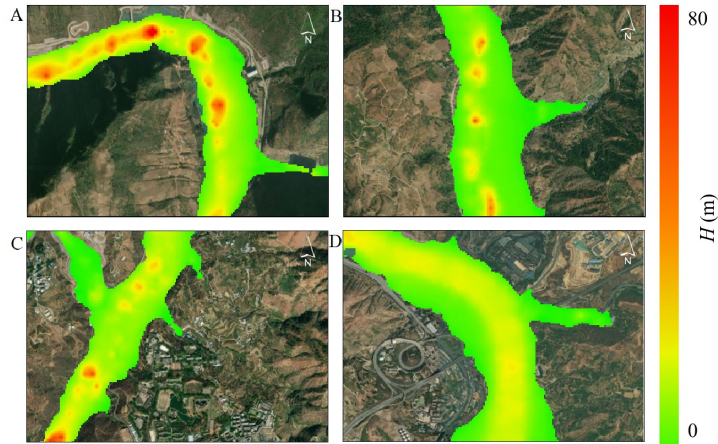


**Figure 14.** Flood depth of representative inundation locations A, B, C, and D under Scenario 4

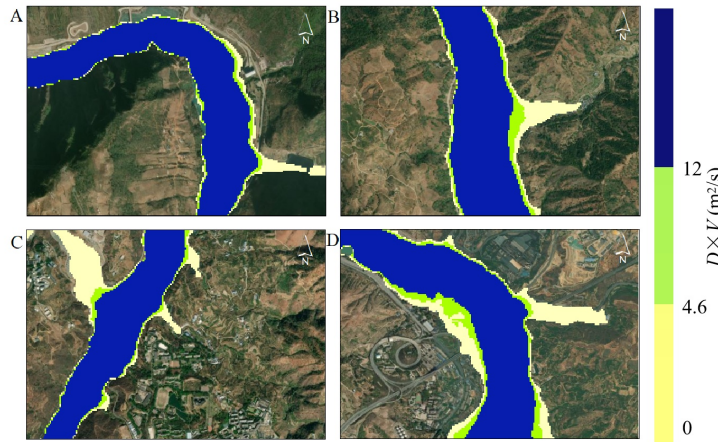


**Figure 15.** Flood inundation degree of representative locations A, B, C, and D under Scenario 4

In Scenario 4, all three reservoirs experienced floods exceeding the standard but did not collapse. According to Figure 14, the maximum submergence depth at representative locations A and C is the highest, reaching 58.23 and 57.37 m respectively. Next is the submerged representative location B, which is 54.67 m. The maximum submergence depth at location D is the smallest, at 31.06 m. At location D, the submerged area is the largest, reaching 1.19 km<sup>2</sup>. The submerged area at point C is the smallest, only 0.73 km<sup>2</sup>.

Therefore, in scenarios 1-3, as the river transitions from the canyon section at point A (with an average slope of 4.2‰) to the impact plain area at point D (with an average slope of 0.7‰), the terrain constraints gradually weaken, and the flood energy shifts from vertical scouring to horizontal diffusion, resulting in a gradual increase in the submerged area of A-D. When all reservoirs experience instantaneous partial collapse (Scenario 1), the peak flood flow at each reservoir is relatively small. When the flood spreads downstream, the maximum flood inundation depth and high severity area in each inundation representative location are also relatively small. In Scenario 3, the reservoirs RE1, RE2, and RE3 all experienced instantaneous full collapse, with larger peak flow rates at each reservoir. When the flood spreads downstream, the water depth and outflow in each representative location are greater. Therefore, compared to Scenarios 1 and 2, Scenario 3 has a larger maximum flood depth and a larger area of high-severity areas at each representative inundation location. In Scenario 3, the maximum flood inundation depths at representative locations A, B, C, and D reached 69.51, 79.87, 77.16, and 48.38 m, respectively. The areas of high-severity zones have reached 0.95, 1.10, 1.21, and 1.73 km<sup>2</sup> respectively. The inundation data for each representative location are shown in Table 6.

Compared to Scenarios 1-3, Scenario 4 has a smaller submerged area at each representative location. Therefore, by improving the flood control safety performance of the dam body, the flood storage can be realized, and the

downstream inundation and flood loss can be reduced. In Scenarios 1-4, significant flooding occurred at locations A, B, C, and D. Special attention should be paid to these areas, and disaster warnings should be made in advance to avoid causing serious losses.

**Table 6.** Maximum water depth and submerged area at each representative location of inundation

Representative Locations	Scenario 1		Scenario 2		Scenario 3		Scenario 4	
	Water depth (m)	Inundated area (km <sup>2</sup> )	Water depth (m)	Inundated area (km <sup>2</sup> )	Water depth (m)	Inundated area (km <sup>2</sup> )	Water depth (m)	Inundated area (km <sup>2</sup> )
A	64.77	0.91	69.51	1.05	69.51	1.05	58.23	0.82
B	68.18	1.12	73.09	1.16	79.87	1.16	54.67	0.90
C	62.53	1.36	67.35	1.53	77.16	1.23	57.37	0.73
D	44.79	1.77	48.78	1.96	48.38	2.05	31.06	1.19

Based on the above inundation analysis results, corresponding flood control and disaster reduction measures are proposed:

(1) For locations A and B, it is recommended to establish a real-time water level monitoring and early warning system to ensure that residents in high-risk areas evacuate 2 hours before the peak of the flood; Implement permanent resettlement in areas with water depths exceeding 50 meters to reduce the risk of casualties.

(2) Due to the fast propagation of flood peaks and wide inundation areas, widening projects need to be implemented in the bends and narrow sections of the river at location C to reduce water blocking effects, and to utilize upstream cascade reservoirs for joint regulation and flood detention.

(3) Due to the flat terrain and large inundation area downstream, it is necessary to establish a flood control system centered on flood storage and detention areas in location D. At the same time, flood channels should be reserved in urban planning to avoid development encroaching on flood discharge space.

#### 4 Conclusions

For the cascade reservoirs of *RE1*, *RE2*, and *RE3*, this study used a hydrodynamic model to simulate the flood process under different breach combination scenarios, revealing the changes in breach water level and flow rate under each breach combination scenario, and comparing and analyzing the depth of flood inundation and the severity of dam breach flood in each representative inundation location. The research results can demonstrate the superposition and peak amplification effects that may be caused by the successive dam failures of cascade reservoirs. The main conclusions are as follows:

(1) In cascade reservoirs, different failure modes of the upstream dam have different impacts on the downstream. Compared with the instantaneous partial collapse mode, the instantaneous full collapse mode will lead to an earlier occurrence time of the flood peak rate after the downstream dam body collapses.

(2) Compared to the single reservoir mode, the flood superposition effect caused by the cascade reservoirs results in a larger and more unfavorable peak flow rate of dam failure at each reservoir when the cascade reservoir group collapses in a chain manner. When the reservoirs *RE1*, *RE2*, and *RE3* all experienced instantaneous full collapse (Scenario 3), the peak flow of dam failure in each reservoir was the highest, reaching 341,200 m<sup>3</sup>/s, 1,157,900 m<sup>3</sup>/s, and 340,100 m<sup>3</sup>/s, respectively.

(3) Compared with Scenarios 1 and 2, Scenario 3 has a larger maximum flood depth, flood inundation area, and high severity area in A, B, C, and D, which is the most unfavorable. In Scenario 3, the maximum submergence depths at representative locations A, B, C, and D are 69.51, 79.87, 77.16, and 48.38 m, respectively. The areas of high-severity zones are 0.95, 1.10, 1.21, and 1.73 km<sup>2</sup>, respectively. When the cascade reservoirs of *RE1*, *RE2*, and *RE3* collapse, efforts should be made to avoid the situation where all three reservoirs collapse instantly to minimize the damage to downstream areas.

In this study, the evolution process of dam failure floods in cascade reservoirs under different failure combination modes was analyzed, but the uncertainty of various risk factors has not yet been considered. In the future work, further consideration will be given to the flood evolution process of cascade reservoirs under both horizontal and vertical breach modes in the CMIP6 climate scenario. At the same time, it can also reveal the impact of different initial water levels on the flood change process of cascade reservoirs, and evaluate the probability of dam failure in each reservoir. The research results can help relevant units develop more targeted emergency response plans, ensuring timely and effective emergency response in the event of a dam failure.

## Author Contributions

Conceptualization, X.Y. Ding; investigation, M.R. Jia; writing-original draft preparation, M.R. Jia, and Xiangyi Ding; writing-review and editing, M.R. Jia, J.Y. Chu, X.Y. Ma, and X.J. Tang. All authors have read and agreed to the published version of the manuscript.

## Funding

This paper was funded by the Major Project of National Natural Science Foundation of China (Grant No.: 52192673); the Major Special Project of “Technology + Water Conservancy” Joint Plan (Grant No.: 2022KSG01007); and Major Science and Technology Project of the Ministry of Water Resources (Grant No.: SKS-2022070).

## Data Availability

The data used to support the findings of this study are available from the corresponding author upon request.

## Conflicts of Interest

The authors declare that there is no conflict of interests regarding the publication of this article.

## References

- [1] T. Wang, Z. H. Li, W. Ge, Y. F. Zhang, Y. C. Jiao, H. R. Sun, and H. Zhang, “Calculation of dam risk probability of cascade reservoirs considering risk transmission and superposition,” *J. Hydrol.*, vol. 609, p. 127768, 2022. <https://doi.org/10.1016/j.jhydrol.2022.127768>
- [2] E. Mühlhofer, E. E. Koks, C. M. Kropf, G. Sansavini, and D. N. Bresch, “A generalized natural hazard risk modelling framework for infrastructure failure cascades,” *Reliab. Eng. Syst. Saf.*, vol. 234, p. 109194, 2023. <https://doi.org/10.1016/j.ress.2023.109194>
- [3] P. C. Larrauri, U. Lall, and R. Zimmerman, “Assessing the hazard from aging dams in the USA,” *Authorea Preprints*, 2022. <https://doi.org/10.1002/essoar.10503795.1>
- [4] J. Liu, T. Song, C. Y. Mei, H. R. Wang, D. Zhang, and S. Nazli, “Flood risk zoning of cascade reservoir dam break based on a 1D-2D coupled hydrodynamic model: A case study on the Jinsha-Yalong River,” *J. Hydrol.*, vol. 639, p. 131555, 2024. <https://doi.org/10.1016/j.jhydrol.2024.131555>
- [5] M. Heidarzadeh and S. Feizi, “A cascading risk model for the failure of the concrete spillway of the Toddbrook dam, England during the August 2019 flooding,” *Int. J. Disaster Risk Reduct.*, vol. 80, p. 103214, 2022. <https://doi.org/10.1016/j.ijdrr.2022.103214>
- [6] W. Liu, P. A. Carling, K. J. Hu, H. R. Wang, Z. Y. Zhou, L. Zhou, and X. W. Zhang, “Outburst floods in China: A review,” *Earth-Sci. Rev.*, vol. 197, p. 102895, 2019. <https://doi.org/10.1016/j.earscirev.2019.102895>
- [7] A. M. Mehta, C. S. Weeks, and E. Tyquin, “Towards preparedness for dam failure: An evidence base for risk communication for downstream communities,” *Int. J. Disaster Risk Reduct.*, vol. 50, p. 101820, 2020. <https://doi.org/10.1016/j.ijdrr.2020.101820>
- [8] H. Tosun and M. A. Hariri-Ardebili, “Post-2023 türkiye earthquake risk assessment of cascade dams in upper Euphrates basin,” *Water Secur.*, vol. 21, p. 100164, 2024. <https://doi.org/10.1016/j.wasec.2023.100164>
- [9] S. Kostecki and R. Banasiak, “The catastrophe of the Niedów dam—the causes of the dam’s breach, its development, and consequences,” *Water*, vol. 13, no. 22, p. 3254, 2021. <https://doi.org/10.3390/w13223254>
- [10] Z. P. Liu, X. L. Guo, X. B. Zhou, H. Fu, Q. F. Xia, and S. J. Li, “Cascading dam breach process simulation using a coupled modeling platform,” *Sci. China Technol. Sci.*, vol. 62, pp. 1455–1466, 2019. <https://doi.org/10.1007/s11431-018-9271-1>
- [11] A. Urzică, A. Mihu-Pintilie, C. C. Stoleriu, C. I. Cîmpianu, E. Huțanu, C. I. Pricop, and A. Grozavu, “Using 2D HEC-RAS modeling and embankment dam break scenario for assessing the flood control capacity of a multi-reservoir system (NE Romania),” *Water*, vol. 13, no. 1, p. 57, 2021. <https://doi.org/10.3390/w13010057>
- [12] J. L. Ma, F. Zhou, C. F. Yue, Q. J. Sun, and X. H. Wang, “The coupled application of the DB-IWHR model and the MIKE 21 model for the assessment of dam failure risk,” *Water*, vol. 16, no. 20, p. 2919, 2024. <https://doi.org/10.3390/w16202919>
- [13] Z. K. Li, W. Li, and W. Ge, “Weight analysis of influencing factors of dam break risk consequences,” *Nat. Hazards Earth Syst. Sci.*, vol. 18, no. 12, pp. 3355–3362, 2018. <https://doi.org/10.5194/nhess-18-3355-2018>
- [14] T. Wang, Z. H. Li, W. Ge, H. Zhang, Y. F. Zhang, H. R. Sun, and Y. C. Jiao, “Risk consequence assessment of dam breach in cascade reservoirs considering risk transmission and superposition,” *Energy*, vol. 265, p. 126315, 2023. <https://doi.org/10.1016/j.energy.2022.126315>
- [15] J. Wang, D. F. Liang, J. X. Zhang, and Y. Xiao, “Comparison between shallow water and boussinesq models for predicting cascading dam-break flows,” *Nat. Hazards*, vol. 83, pp. 327–343, 2016. <https://doi.org/10.1007/s11069-016-2317-x>

- [16] J. Říha, S. Kotaška, and L. Petrula, “Dam break modeling in a cascade of small earthen dams: Case study of the Čižina River in the Czech Republic,” *Water*, vol. 12, no. 8, p. 2309, 2020. <https://doi.org/10.3390/w12082309>
- [17] T. Wang, Z. K. Li, W. Ge, Y. D. Zhang, Y. T. Jiao, H. Zhang, H. Q. Sun, and P. van Gelder, “Risk assessment methods of cascade reservoir dams: A review and reflection,” *Nat. Hazards*, vol. 115, no. 2, pp. 1601–1622, 2023. <https://doi.org/10.1007/s11069-022-05609-z>
- [18] T. Liu, “Numerical simulation on dam-break flooding of cascade reservoirs in the Yalong River Basin,” Master’s thesis, China Three Gorges University, 2019.
- [19] G. W. Brunner, *HEC-RAS river analysis system: Hydraulic reference manual*, Hydrologic Engineering Center, Davis, California, 1997, version 1.0.
- [20] M. Beza, A. Fikre, and A. Moshe, “Dam breach modeling and downstream flood inundation mapping using HEC-RAS model on the proposed Gumara dam, Ethiopia,” *Adv. Civ. Eng.*, vol. 2023, no. 1, p. 8864328, 2023. <https://doi.org/10.1155/2023/8864328>
- [21] C. X. Mo, Y. Shen, X. B. Lei, H. Z. Ban, Y. L. Ruan, S. F. Lai, and Z. X. Xing, “Simulation of one-dimensional dam-break flood routing based on HEC-RAS,” *Front. Earth Sci.*, vol. 10, p. 1027788, 2023. <https://doi.org/10.3389/feart.2022.1027788>
- [22] I. Gabriel-Martin, A. Sordo-Ward, L. Garrote, and L. G. Castillo, “Influence of initial reservoir level and gate failure in dam safety analysis. Stochastic approach,” *J. Hydrol.*, vol. 550, pp. 669–684, 2017. <https://doi.org/10.1016/j.jhydrol.2017.05.032>
- [23] X. Liu, M. X. Yang, X. Y. Meng, F. Wen, and G. D. Sun, “Assessing the impact of reservoir parameters on runoff in the Yalong River Basin using the SWAT model,” *Water*, vol. 11, no. 4, p. 643, 2019. <https://doi.org/10.3390/w11040643>
- [24] P. Ren, J. Zhou, L. Mo, and Y. D. Zhang, “Comprehensive study on cascade hydropower stations in the lower reaches of Yalong River for power generation and ecology,” *Energy Sustain. Dev.*, vol. 73, pp. 236–246, 2023. <https://doi.org/10.1016/j.esd.2022.12.013>